Journal of Electroanalytical Chemistry 855 (2019) 113598

Contents lists available at ScienceDirect

Journal of Electroanalytical Chemistry

journal homepage: www.elsevier.com/locate/jelechem

Using a multiway chemometric tool in the evaluation of methanol electro-oxidation mechanism

Camila D. Silva [a], Patricia G. Corradini [a], Lucia H. Mascaro [a], Sherlan Lemos [b], Ernesto C. Pereira [a,*]

[a] Department of Chemistry, Federal University of São Carlos, Rod.Washington Luiz, km 235, CEP 13565-905 São Carlos, SP, Brazil
[b] Department of Chemistry, Federal University of Paraíba, C.P. 5093, 58051-970, João Pessoa, PB, Brazil

ARTICLE INFO

Keywords:
Methanol oxidation reaction
PARAFAC
ATR-SEIRAS
Mechanism
Platinum

ABSTRACT

In the present work, an innovative methodology is used to contribute in the elucidation of methanol electro-oxidation reaction on polycrystalline Pt surface. We coupled infrared spectroscopy to linear voltammetry and evaluate the data using parallel factor analysis (PARAFAC) to extract hidden information concerning the oxidation reaction. Five adsorbed species were simultaneously extracted and quantified at different applied potentials corresponding to: formate, sulfate, water, total CO and COL shift. It was observed that the CO adsorbed content starts at maximum on low potentials and gradually decreases up to 1.0 V. Meanwhile, the interfacial water content on the surface of the CO-free Pt increases, which causes the shift on the CO_L band, resulting in a further decrease of the interfacial water content. The water content increases again until up to 0.8 V, which it reaches a constant value, due to formate production and subsequent adsorption of sulfate. Using this technique, it was possible to determine the potential window where each chemical species is adsorbed on the surface, as well as the effect of methanol concentration and scan rate on the mechanism.

1. Introduction

The electro-oxidation of small organic alcohols, such as methanol and ethanol, has been studied extensively over the years because their importance in the development of direct alcohol fuel cells [1–6]. Methanol has been highlighted from other liquid fuels due the possibility of its complete oxidation, generating CO_2 [7]. However, methanol electro-oxidation reaction (MOR) over platinum electrodes involve several steps, which are reaction intermediates or catalytic poisons, depending on the adsorption energy. The majority of works in the literature reports the usage of electrochemical techniques coupled to spectroscopic ones to investigate the reaction mechanism, such as on-line electrochemical mass spectrometry and Fourier-transform infrared spectroscopy (FTIR) [8–12]. Although in situ techniques allow the detection of different species, it is very difficult to correlate the reaction products with the common electrochemical responses, as, for example, current-time, polarization or cyclic voltammetric curves, due to overlapping processes. This is especially true considering FTIR technique. Indeed, the correlation among the identified species and electrochemical results is not a trivial task and, until now, this relationship has been not totally clarified [3,11].

Considering the difficulty to split the contribution of the different step involved in both electrochemical responses and FTIR data, it is important to look for experimental or computational tools to get the complete information relating these different techniques. One possibility is chemometrics, which has been shown to improve the treatment of chemical data [13–17]. In this sense, parallel factor analysis (PARAFAC) is highlighted in data processing for being very simple in a mathematical sense, robust and the results can be easily understandable [14,15,18,19]. PARAFAC is a generalization of principal component analysis (PCA) for multiway data or can even be described as a less flexible version of the Tucker 3 method [19,20]. In a sense, PARAFAC can be considered as hard modelling, since it is suitable for the analysis of systems with variables clearly defined by physical-chemical laws [13,19–21]. This technique has been proposed for modelling trilinear three-way data $\boldsymbol{X}$ (experimentally measured signals), which could be described as following [22]:

$$x_{ijk} = \sum_{n=1}^{N} a_{in} b_{jn} c_{kn} + e_{ijk} \quad (1)$$

where x_{ijk} is an element of $\boldsymbol{X}$, a_{in} denotes the values of the profile in the

* Corresponding author.
E-mail address: ernesto@ufscar.br (E.C. Pereira).

https://doi.org/10.1016/j.jelechem.2019.113598
Received 4 July 2019; Received in revised form 26 September 2019; Accepted 21 October 2019
Available online 1 November 2019

sample mode for constituent n in sample i, and b_{jn} and c_{kn} are the corresponding profile values in both instrumental data modes for constituent n, with e_{ijk} representing the model errors (unavoidable measurements noise). Modelling $\boldsymbol{X}$ through PARAFAC consists in fit the x_{ijk} elements and retrieve the values of a_{in}, b_{jn}, and c_{kn} through alternate least-squares by minimizing the sum of the squared errors (SSE):

$$\mathrm{SSE} = \sum_{i=1}^{I}\sum_{j=1}^{J}\sum_{k=1}^{K} e_{ijk}^2 \tag{2}$$

To make clear the ideas underneath PARAFAC, Fig. 1 illustrates data processing by PARAFAC algorithm. PARAFAC modelling obtains triads of vectors related to each component of the system, generating a unique solution for a certain number of components. It is customary to arrange them into three matrices: the matrix of scores A (size I x N, containing all a_{in} values), and the two matrices of loadings B (size N x J, containing all b_{jn} values), and C (size K x N, containing all c_{kn} values).

PARAFAC can be easily implemented since this algorithm is available free of charge in toolboxes elaborated for Matlab® (Mathworks) environment [23,24]. This tool has been used in excitation–emission matrix (EEM) fluorescence spectra [25–27], gas chromatography with mass spectra detection (GC-MS) [28], high-performance liquid chromatography (HPLC) [29] and for ultraviolet–visible (UV–Vis) and near infrared (NIR) spectroscopy [30]. In the FTIR case, PARAFAC tool is especially suitable for mechanism elucidation but is not a widely used tool, and, to the best of our knowledge, has not be used to investigate electrocatalytical data.

In this sense, the aim of this paper is to use this multiway chemometric tool to extract the latent information regarding electrochemical and FTIR spectroscopic data for methanol oxidation reaction (MOR) on polycrystalline platinum surface.

2. Experimental section

The study of MOR on polycrystalline platinum was performed using attenuated total reflectance surface-enhanced infrared absorption spectroscopy (ATR-SEIRAS) experiments. The fundamental aspects of this technique have been described in Refs. [31,32]. The working solutions were prepared from concentrated H_2SO_4 (Fluka, trace select, for trace analysis) and ultra-pure water (18.2 MΩ cm). The solutions were desaerated with nitrogen (99.0%, White Martins®) before the experiments. A Pt wire and a reversible hydrogen electrode (RHE) were used as counter and reference electrodes, respectively. A potentiostat (Em Stat, Palm Sens®) was used to control electrode potential and to record linear voltammograms. ATR-SEIRAS spectra were recorded with a Nicolet 6700 FTIR spectrometer equipped with an MCT detector, using p-polarized light. The prism for the ATR-SEIRAS measurements was a triangular Si crystal 4.00 cm^2 in area.

A Pt film deposited on the triangular Si prism by chemical deposition was the working electrode. Before chemical deposition, the Si substrate surface was polished with alumina powder (1.00 μm grade) and cleaned with acetone and water. First, to improve the adhesion of the Pt film to the substrate, the polished surface was treated with Pd solution (1 mmol L^{-1} $PdCl_2$ in 0.5% HF) at room temperature for ca. 1.5 min [33]. Then, Pt film was deposited using a Pt plating solution, which was dropped on the prism surface for approximately 3 min at 60–70 °C temperature. The Pt plating bath was prepared using the procedure described in the literature [34].

Before the ATR-SEIRAS experiments, the Pt surface was electrochemically cleaned by repetitive potential cycling between 0.05 and 1.5 V *vs.* RHE in the supporting electrolyte (0.1 mol L^{-1} H_2SO_4). The spectral series were simultaneous recorded with the linear sweep voltammetry (LSV) in order to identify the intermediates and products reaction. Each spectrum consisted of 15 interferograms, collected with a spectral resolution of 8 cm^{-1}. The reference spectrum consisted of 64 interferograms and was recorded in the absence of methanol in the potential 0.05 V before each simultaneous methanol electro-oxidation and IR experiments. The procedure was aimed at recovering the unique spectra of each species formed during MOR and correlate them to the respective absorption profile as a function of the applied potential sweep.

Referring to Fig. 1, in this paper the horizontal slice on $\boldsymbol{X}$ represents a second-order data array obtained by performing one ATR-SEIRAS/LSV

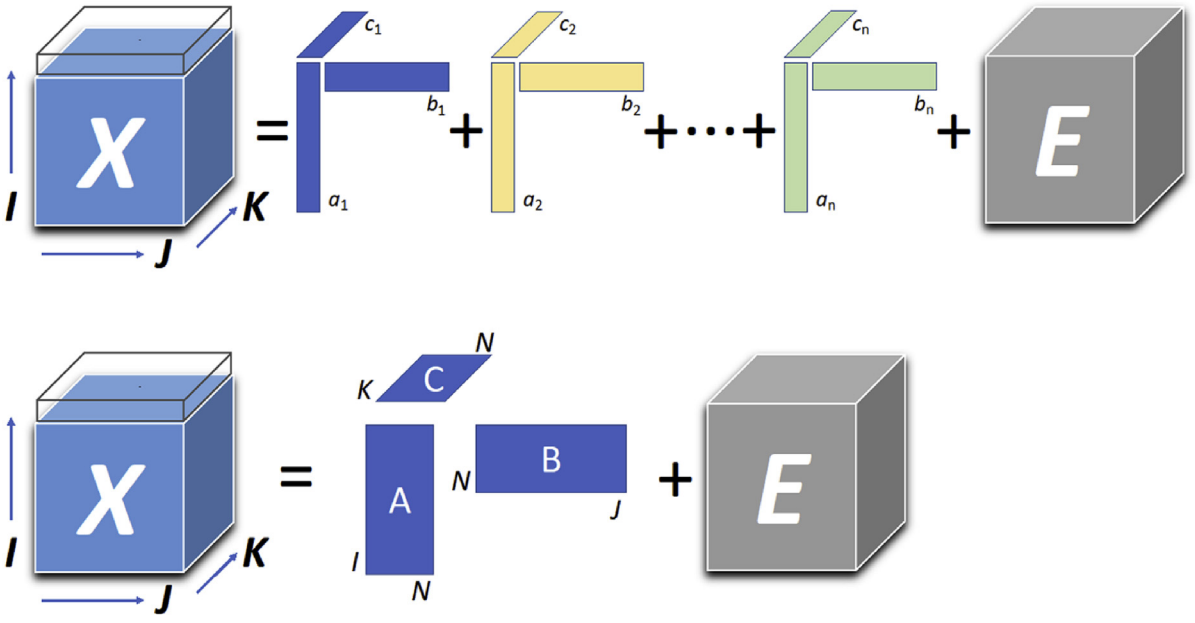

Fig. 1. Illustrative representation of PARAFAC algorithm. Decomposition of a three-way array data $\boldsymbol{X}$ in n triads of vectors. Matrix A contains scores for I experiments; matrix B and C contain loadings for modes J and K (FTIR spectra and voltoabsorptiograms, respectively); E contains the residuals. The horizontal slice on $\boldsymbol{X}$ represents a second-order data array obtained by performing one ATR-SEIRAS/LSV experiment.

experiment. To build the three-way array data ***X***, ATR-SEIRAS/LSV experiments were executed following a 2^2-factorial design containing the variables methanol concentration and LSV scan rate. The low and high levels for each variable were, respectively, 0.5 mol L^{-1} and 1.0 mol L^{-1} for methanol concentration, and 5 mV s^{-1} and 10 mV s^{-1} for scan rate. The four combinations were carried out in duplicate, comprising eight experiments, presented at Table 1.

3. Results and discussion

To characterize Pt surface, cyclic voltammetry measurements were carried out. Fig. S1 in the Supporting Information (SI) shows the platinum characteristic profile in acid medium is observed, proving the cleaning of the electrode and the electrochemical cell. After methanol addition, a LSV curve was obtained (Fig. 2a). During the oxidation of methanol, the most accepted model correlates the first reaction step, up to 0.4 V (*vs*. RHE), to the dehydrogenation producing HCOH, and/or CO species [8,35–37]. At 0.9 V (*vs*. RHE), HCOOH and CO_2 are proposed to form. However, the analysis of the curve peaks is a hard work, since different intermediates can be simultaneously formed during this process, such as CO, CO_2, HCOOH, HCOH and $HCOOCH_3$ [12,35,38,39]. The ATR-SEIRAS data support the above propositions (Fig. 2b). In Fig. S2 in SI is presented the ATR-SEIRAS for all studied condition, listed at Table 1. Following literature description, the major bands are identified in Table 2.

Scores matrix carry information on concentrations of N constituents in each experiment ($I = 8$), whereas loadings matrices provide a qualitative insight into the behavior of the constituents in the instrumental measurement modes – N spectra with J wavenumbers, and N voltoabsorptiograms with K applied potentials. The factorial design was employed using two variables (methanol concentration and scanning speed) in order to determine the influence of these variables on the concentration variation of each species produced as an intermediate of the methanol electro-oxidation reaction.

The first attempts of data analysis consisted on find the unique spectrum of each of the seven bands originally assigned at Table 2. However, modelling results always were composed of random noise profiles and/or repeated profiles, which indicate that the correct number of components was less than seven. Satisfactory results were only obtained when five components were employed. Fig. 3a shows the outputs of loadings matrix B (spectral profiles), in other words, the statistically significant signals that compose the ATR/SEIRAS response. Component #1 showed a profile with a peak at 1230 cm^{-1}, similar to the stretch of adsorbed sulfate. The profile of component #2 has a maximum at 1320 cm^{-1}, which can be attributed to formate vibration. Component #3 presented a profile with minimum at 3510 cm^{-1}, which is very similar to the OH stretch of interfacial water (ν^*_{OH}) on Pt surface. No pure spectra were found that could be attributed to OH stretch of interfacial water (ν_{OH}) and to δ(HOH) – around 3670 cm^{-1} and 1620 cm^{-1}, respectively – which could be related to the low signal-to-noise ratio presented for both bands. Component #4 presented a profile with a peak at 2060 cm^{-1}, while the component #5 has a more complex profile containing a band with maximum at 2050 cm^{-1} and a plateau between 1780 and 1970 cm^{-1}. These two last components could be related to CO species, at linear and bridge forms. In this case it was not possible to split the spectral information of the two CO adsorbed forms in two specific bands. Otherwise, it was possible to attribute components #4 and #5 to the total adsorbed CO and to the shift of the band related to CO_L adsorbed species. This is an important observation because the most common approach to explain the MOR mechanism is by correlating it to the kind of CO-adsorbed layer [37,40–44].

Table 1
Design matrix followed for the execution of the ATR-SEIRAS/LSV experiments.

Experiment #	Scan rate (mV s^{-1})	Methanol concentration (mol L^{-1})
1	5	0.5
2	5	0.5
3	10	0.5
4	10	0.5
5	5	1.0
6	5	1.0
7	10	1.0
8	10	1.0

In an effort to understand how these components could be described, it is observed that the CO_L band presented a shift during the potential sweep. The contour plot of this band is given in Fig. 3b. The CO_L band shift is a phenomenon observed in other papers about alcohol oxidation [12,38,45–47]. This displacement could be correlated to changes in dipole-dipole interactions [48] and to the vibrational Stark effect [49]. Kim et al. [48] explained the potential-dependent of dipole-dipole interactions to the metal, which affect CO ad-layers structures. The authors proposed that hydrogen co-adsorption can weaken CO intermolecular coupling, since the hydrogen ad-layer reduces the magnitude of the dipole-dipole coupling interactions [48]. Boscheto et al. [50] reported the dynamic oscillatory behavior of methanol oxidation, and explained that dipole-dipole interaction is more pronounced for CO_L coverage, while the vibrational Starks effect influences the CO_L band position. Although these effects were reported, the CO_L band shift was not addressed to MOR mechanism. Against this backdrop, we can understand component #4 (Fig. 3a) as a blue shift of CO_L band during LSV and component #5 as the all CO-adsorbed contribution (CO_B + CO_L).

Fig. 4a shows the outputs of loadings matrix C, i.e., the behavior of the spectra identified at Fig. 3a, as a function of the voltammetric scan (voltoabsorptiograms). CO_{ad} curve (CO_B + CO_L) starts at a maximum value, indicating of high coverage of CO_{ad} at low potentials. The increment of potential reduces the total CO_{ad} band intensity, promoted by CO oxidation at low potentials. No CO_{ad} absorption was observed at potentials more positive than 1.0 V, which is a potential sufficient to promote the rapid oxidation of this species, disfavoring its adsorption. The green curve (CO_L shift) begins at 0.25 V and reaches a maximum at 0.6 V, which indicates the influence of potential sweep on the shift of CO_L band. After 0.6 V, the CO_L-shifted band decreased to zero intensity at 0.85 V. The formate band appears at potentials more positive than 0.7 V, reaching a maximum at 0.9 V, and decreasing to a minimum value at 1.1 V. Sulfate keeps the same intensity around all potential range, only increasing after 1.2 V. This fact illustrates the adsorption force of this species, already reported by different works [51–54].

For methanol oxidation, the water dissociation is described as an important step due this importance for oxygen donor of the reaction [36,55,56]. Regarding water adsorption, the associated profile presented a band with negative values. This means that the curve should be analyzed differently from previous components. At low potentials, the OH-coverage is small, but increases until 0.4 V, and, then, begins to decrease, reaching the minimum intensity around 0.65 V. Iwasita explained that competition of water and methanol for adsorption sites becomes important as the potential is made more positive, especially at 0.4 V–0.7 V [55,57]. After this potential, OH-coverage increases again up to 0.8 V, where it remains approximately constant. Considering the information that each profile represents, it can be said that the CO adsorbed content starts at maximum and gradually decreases up to 1.0 V. Meanwhile, the interfacial water content on the surface of the CO-free Pt increases, which causes the shift on the CO_L band, resulting in a further decrease of the interfacial water content, what is described by Langmuir-Hinschelwood mechanism, for CO_2 formation [55,58]. The water content increases again until it reaches a constant value due to formate production and subsequent adsorption of sulfate. Fig. 5 provides an illustration of MOR mechanism on Pt surface.

In the literature, the MOR kinetic is common correlated to the shape, composition and size of particle, while the effect of the experimental variables (scan rate and methanol concentration) are not evaluated in recent works [11]. These variables deserve attention when evaluating the mechanism, since adsorbed composition on platinum depends on

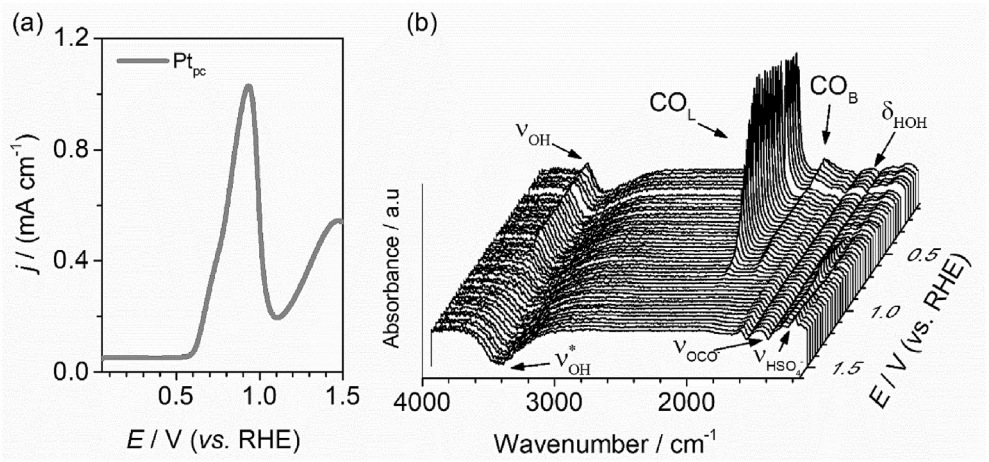

Fig. 2. Investigation of methanol oxidation reaction (MOR) in polycrystalline Pt (Pt_{pc}): (a) LSV curve of methanol 0.5 mol L^{-1} in H_2SO_4 0.1 mol L^{-1} at Pt_{pc} (scan rate: 5 mV s^{-1}, T = 25 °C, current density normalized by geometrical area). (b) ATR-SEIRAS spectra recorded simultaneously to linear sweep voltammetry.

Table 2
Assignment of the bands observed in the ATR-SEIRAS measurements [38].

ν/cm^{-1}	Description
3670	OH stretching of interfacial water (ν_{OH})
3510	OH stretching of interfacial water (ν^*_{OH}) on Pt surface without CO
2060	CO linear (CO_L)
1840	CO brigde (CO_B)
1620	H–O–H twist (δ_{HOH})
1320	Formate stretching (ν_{OCO^-})
1230	Adsorbed sulfate ($\nu_{HSO_4^-}$) on Pt

methanol concentration and that dependence could explained some discrepancies of results in the literature [36,55,59]. Fig. 4b shows the average PARAFAC scores (outputs of matrix A) obtained for each component at each experiment of the 2^2-factorial design. It is important to note that profiles at loadings matrices are normalized to unit length, leaving the concentration-dependent scaling factor to the a_{in} elements of matrix A. In this work, the element a_{in} will be proportional to the concentration of component n in each experiment. Therefore, an analysis of variance (ANOVA) was performed in the scores to infer whether the scan rate or the methanol concentration show any influence on the concentrations of the species throughout the experiments. Pareto charts are presented on Fig. 6. The Pareto chart is a graphical representation of a t-statistic test for each effect. Each bar is proportional to the standardized effect, which is the estimated effect divided by its standard error, presented in decreasing order of importance. The vertical line is used to judge which effects are statistically significant at 95% confidence level. Any bar which extend beyond the line corresponds to the effects which are statistically significant for the change of the concentration of the component. Methanol concentration and scan rate presented no significant influence on OH and sulfate concentrations. Some authors comment that in methanol concentrations between 0.1 and 0.5 mol L^{-1}, there is a higher probability of the Pt surface becomes covered for CO, and hydrogen adsorbed species is inhibited due to the lack of free adjacent sites [2,57]. However, the methanol concentration increment, to 1.0 mol L^{-1}, presented a negative effect for formate, CO_L shift and CO-total. It means that the concentrations of adsorbed formate and CO decrease with increasing concentration of methanol. The same occurs for scan rate on the concentration of adsorbed CO species. It appears that a higher methanol concentration hinders the adsorption of that species. Higher scan rates also promote the decreasing of the amount of adsorbed CO, indicating that the dynamical balance of the species could be affected by the evolution of the MOR [47,50,60].

4. Conclusion

The main idea of this paper was to report, for the first time, the usage of a multiway chemometric tool, PARAFAC, to contribute to the elucidation of MOR oxidation mechanism on Pt surface. Five components associated to intermediate species were calculated from ATR-SEIRAS/LSV data: formate, sulfate, water, CO total and CO_L shift. We also conclude that changing common experimental conditions during the electrochemical experiments, such as methanol concentration and scan rate, could affect the surface concentration of the intermediates. Finally,

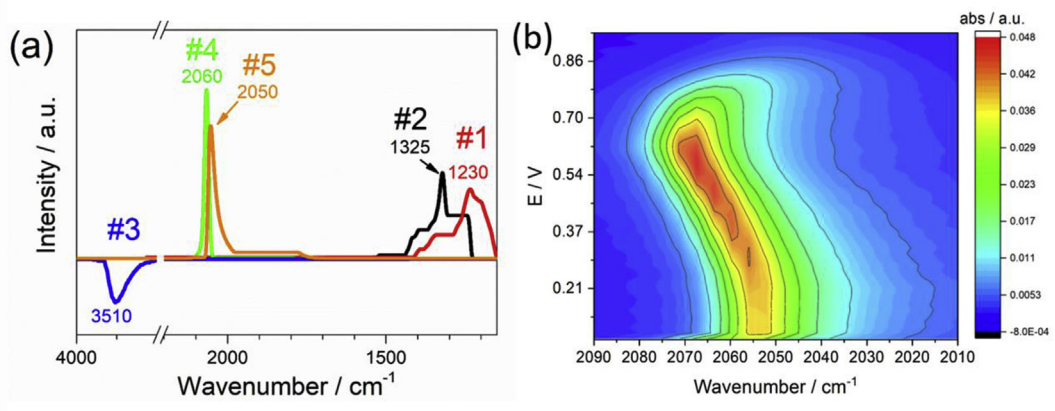

Fig. 3. (a) Spectral profiles of the components obtained after PARAFAC analysis of ATR-SEIRAS/LSV data. (b) CO_L band shift at ATR-SEIRAS experiments during LSV.

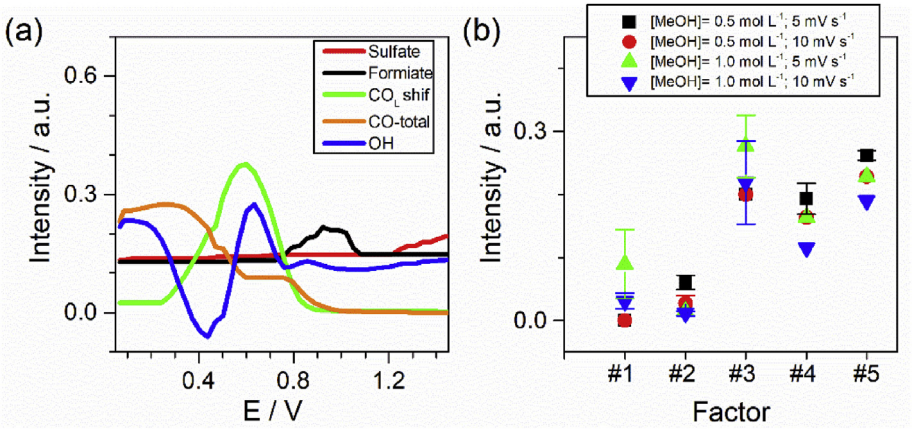

Fig. 4. (a) Voltoabsorptiograms of the five components. (b) Average PARAFAC scores obtained for each component at the experiments of the 2^2-factorial design. #1: sulfate; #2: formate; #3: water; #4: CO_L shift; #5: CO-total.

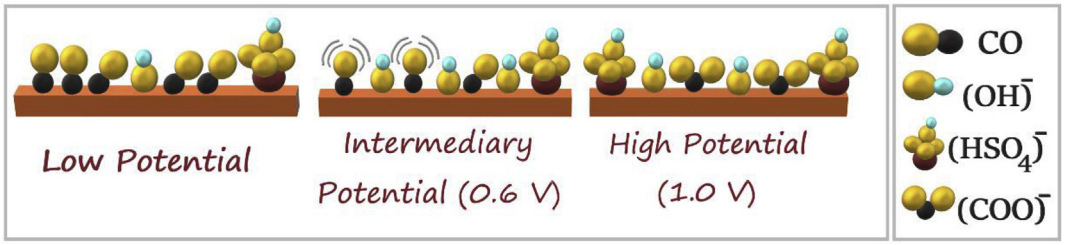

Fig. 5. Illustrative scheme of the mechanism of methanol oxidation reaction.

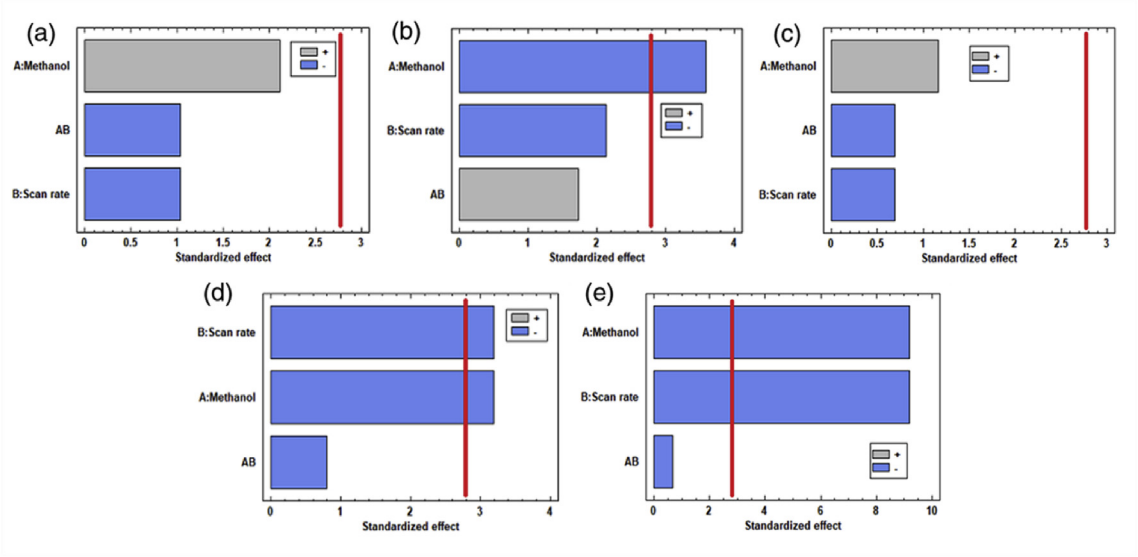

Fig. 6. Pareto charts for the analysis of variance of the PARAFAC scores as responses to the 2^2-factorial design for (a) #1 (sulfate); (b) #2 (formate); (c) #3 (water); (d) #4 (CO_L shift) and, (e) #5 (CO-total). Gray bars: positive effect. Blue bars: negative effect.

this work shows that PARAFAC can be used to investigate the oxidation of different small organic molecules, which are important in the development of on electrochemical energy conversion devices.

Associated content

Supporting Information. The following files are available free of charge: Cyclic voltammetry of Pt_p and ATR-SEIRAS spectra for all studied conditions.

Notes

The authors declare no competing financial interests.

Acknowledgments

The authors thank the São Paulo Research Foundation (FAPESP) for financial assistance to the project granted (FAPESP/CDMF #2013/07296-2 and FAPESP/GSK #2014/50249-8). The authors also thank to

the Coordenação de Aperfeiçoamento de Pessoal de Nível Superior - Brasil (CAPES) - Finance Code 001 and by Conselho Nacional de Pesquisa e Desenvolvimento (CNPq, #143341/2014-6, #167430/2017-3, #152303/2018-9), for fellowships granted.

Appendix A. Supplementary data

Supplementary data to this article can be found online at https://doi.org/10.1016/j.jelechem.2019.113598.

References

[1] H. Hitmi, E.M. Belgsir, J.M. Léger, C. Lamy, R.O. Lezna, A kinetic analysis of the electro-oxidation of ethanol at a platinum electrode in acid medium, Electrochim. Acta 39 (1994) 407–415, https://doi.org/10.1016/0013-4686(94)80080-4.
[2] T. Iwasita, E. Pastor, A DEMS and FTIR spectroscopic investigation of adsorbed ethanol on polycrystalline platinum, Electrochim. Acta 39 (1994) 531–537, https://doi.org/10.1016/0013-4686(94)80097-9.
[3] M. Neurock, M. Janik, A. Wieckowski, A first principles comparison of the mechanism and site requirements for the electrocatalytic oxidation of methanol and formic acid over Pt, Faraday Discuss 140 (2009) 363–378, https://doi.org/10.1039/B804591G.
[4] E. Antolini, Platinum-based ternary catalysts for low temperature fuel cells Part I. Preparation methods and structural characteristics, Appl. Catal. B Environ. 74 (2007) 324–336, https://doi.org/10.1016/j.apcatb.2007.03.002.
[5] E. Antolini, Platinum-based ternary catalysts for low temperature fuel cells Part II. Electrochemical properties, Appl. Catal. B Environ. 74 (2007) 337–350, https://doi.org/10.1016/j.apcatb.2007.03.001.
[6] Y. Wang, S.Z. Zou, W.B. Cai, Recent advances on electro-oxidation of ethanol on Pt- and Pd-based catalysts: from reaction mechanisms to catalytic materials, Catalysts 5 (2015) 1507–1534, https://doi.org/10.3390/catal5031507.
[7] J.-M. Léger, Mechanistic aspects of methanol oxidation on platinum-based electrocatalysts, J. Appl. Electrochem. 31 (2001) 767–771, https://doi.org/10.1023/A:1017531225171.
[8] T. Iwasita, W. Vielstich, On-line mass spectroscopy of volatile products during methanol oxidation at platinum in acid solutions, J. Electroanal. Chem. Interfacial Electrochem. 201 (1986) 403–408, https://doi.org/10.1016/0022-0728(86)80064-X.
[9] R. Ortiz, O.P. Márquez, J. Márquez, C. Gutiérrez, Necessity of oxygenated surface species for the electrooxidation of methanol on iridium, J. Phys. Chem. 100 (1996) 8389–8396, https://doi.org/10.1021/jp953185i.
[10] T.H.M. Housmans, A.H. Wonders, M.T.M. Koper, Structure sensitivity of methanol electrooxidation pathways on Platinum: an on-line electrochemical mass spectrometry study, J. Phys. Chem. B 110 (2006) 10021–10031, https://doi.org/10.1021/jp055949s.
[11] L. Gong, Z. Yang, K. Li, W. Xing, C. Liu, J. Ge, Recent development of methanol electrooxidation catalysts for direct methanol fuel cell, Journal of Energy Chemistry 27 (2018) 1618–1628, https://doi.org/10.1016/j.jechem.2018.01.029.
[12] W. Chen, J. Cai, J. Yang, M.M. Sartin, Y.-X. Chen, The kinetics of methanol oxidation at a Pt film electrode, a combined mass and infrared spectroscopic study, J. Electroanal. Chem. 800 (2017) 89–98, https://doi.org/10.1016/j.jelechem.2017.01.011.
[13] M.M. Sena, M.G. Trevisan, R.J. Poppi, PARAFAC: uma ferramenta quimiométrica para tratamento de dados multidimensionais. Aplicações na determinação direta de fármacos em plasma humano por espectrofluorimetria, Quím. Nova 28 (2005) 910–920, https://doi.org/10.1590/S0100-40422005000500032.
[14] E. Szymańska, J. Gerretzen, J. Engel, B. Geurts, L. Blanchet, L.M.C. Buydens, Chemometrics and qualitative analysis have a vibrant relationship, Trac. Trends Anal. Chem. 69 (2015) 34–51, https://doi.org/10.1016/j.trac.2015.02.015.
[15] Y.-P. Wang, Y.-R. Zou, J.-T. Shi, J. Shi, Review of the chemometrics application in oil-oil and oil-source rock correlations, Journal of Natural Gas Geoscience 3 (2018) 217–232, https://doi.org/10.1016/j.jnggs.2018.08.003.
[16] A. Omidvarnia, G. Azemi, P.B. Colditz, B. Boashash, A time–frequency based approach for generalized phase synchrony assessment in nonstationary multivariate signals, Digit. Signal Process. 23 (2013) 780–790, https://doi.org/10.1016/j.dsp.2013.01.002.
[17] P. Calza, V.A. Sakkas, C. Medana, A.D. Vlachou, F. Dal Bello, T.A. Albanis, Chemometric assessment and investigation of mechanism involved in photo-Fenton and TiO2 photocatalytic degradation of the artificial sweetener sucralose in aqueous media, Appl. Catal. B Environ. 129 (2013) 71–79, https://doi.org/10.1016/j.apcatb.2012.08.043.
[18] R.A. Harshman, M.E. Lundy, PARAFAC: parallel factor analysis, Comput. Stat. Data Anal. 18 (1994) 39–72, https://doi.org/10.1016/0167-9473(94)90132-5.
[19] R. Bro, PARAFAC. Tutorial and applications, Chemometrics and Intelligent Laboratory Systems 38 (1997) 149–171, https://doi.org/10.1016/S0169-7439(97)00032-4.
[20] L.R. Tucker, Some mathematical notes on three-mode factor analysis, Psychometrika 31 (1966) 279–311, https://doi.org/10.1007/BF02289464.
[21] N.M. Faber, R. Bro, P.K. Hopke, Recent developments in CANDECOMP/PARAFAC algorithms: a critical review, Chemometr. Intell. Lab. Syst. 65 (2003) 119–137, https://doi.org/10.1016/S0169-7439(02)00089-8.
[22] R.B. Martí, J.F. Baldrich, Fundamentals of PARAFAC, in: A.M. de la Peña, H.C. Goicoechea, G.M. Escandar, A.C. Olivieri (Eds.), Data Handling in Science and Technology, Elsevier, 2015, pp. 7–35.
[23] C.A. Andersson, R. Bro, The N-way toolbox for MATLAB, Chemometr. Intell. Lab. Syst. 52 (2000) 1–4, https://doi.org/10.1016/S0169-7439(00)00071-X.
[24] A.R. Jalalvand, M. Roushani, H.C. Goicoechea, D.N. Rutledge, H.-W. Gu, MATLAB in electrochemistry: a review, Talanta 194 (2019) 205–225, https://doi.org/10.1016/j.talanta.2018.10.041.
[25] J. Costa Pereira, A.A.C.C. Pais, H.D. Burrows, Analysis of raw EEM fluorescence spectra - ICA and PARAFAC capabilities, Spectrochim. Acta A Mol. Biomol. Spectrosc. 205 (2018) 320–334, https://doi.org/10.1016/j.saa.2018.07.025.
[26] M. Steiner-Browne, S. Elcoroaristizabal, Y. Casamayou-Boucau, A.G. Ryder, Investigating native state fluorescence emission of Immunoglobulin G using polarized Excitation Emission Matrix (pEEM) spectroscopy and PARAFAC, Chemometr. Intell. Lab. Syst. 185 (2019) 1–11, https://doi.org/10.1016/j.chemolab.2018.12.007.
[27] D.A. Gordon, Z. Zhan, L.S. Bruckman, Characterizing the weathering induced degradation of Poly(ethylene-terephthalate) using PARAFAC modeling of fluorescence spectra, Polym. Degrad. Stab. 161 (2019) 85–94, https://doi.org/10.1016/j.polymdegradstab.2019.01.006.
[28] L. Rubio, L. Valverde-Som, L.A. Sarabia, M.C. Ortiz, The behaviour of Tenax as food simulant in the migration of polymer additives from food contact materials by means of gas chromatography/mass spectrometry and PARAFAC, J. Chromatogr. A 1589 (2019) 18–29, https://doi.org/10.1016/j.chroma.2018.12.054.
[29] F.C. Guizellini, G.G. Marcheafave, M. Rakocevic, R.E. Bruns, I.S. Scarminio, P.K. Soares, PARAFAC HPLC-DAD metabolomic fingerprint investigation of reference and crossed coffees, Food Res. Int. 113 (2018) 9–17, https://doi.org/10.1016/j.foodres.2018.06.070.
[30] L.N. Rosa, A. Coqueiro, P.H. Março, P. Valderrama, Thermal rice oil degradation evaluated by UV–Vis-NIR and PARAFAC, Food Chem. 273 (2019) 52–56, https://doi.org/10.1016/j.foodchem.2018.03.065.
[31] A.R. Hind, S.K. Bhargava, A. McKinnon, At the solid/liquid interface: FTIR/ATR — the tool of choice, Adv. Colloid Interface Sci. 93 (2001) 91–114, https://doi.org/10.1016/S0001-8686(00)00079-8.
[32] C.D. Silva, G. Cabello, W.A. Christinelli, E.C. Pereira, A. Cuesta, Simultaneous time-resolved ATR-SEIRAS and CO-charge displacement experiments: the dynamics of CO adsorption on polycrystalline Pt, J. Electroanal. Chem. 800 (2017) 25–31, https://doi.org/10.1016/j.jelechem.2016.10.034.
[33] R.G. Freitas, E.P. Antunes, P.A. Christensen, E.C. Pereira, The influence of Ir and Pt1Ir1 structure in metallic multilayers nanoarchitectured electrodes towards ethylene glycol electro-oxidation, J. Power Sources 214 (2012) 351–357, https://doi.org/10.1016/j.jpowsour.2012.04.099.
[34] J.N. Tiwari, R.N. Tiwari, G. Singh, K.S. Kim, Recent progress in the development of anode and cathode catalysts for direct methanol fuel cells, Nano Energy 2 (2013) 553–578, https://doi.org/10.1016/j.nanoen.2013.06.009.
[35] T. Zerihun, P. Grundler, Oxidation of formaldehyde, methanol, formic acid and glucose at ac heated cylindrical Pt microelectrodes, J. Electroanal. Chem. 441 (1998) 57–63, https://doi.org/10.1016/S0022-0728(97)00400-2.
[36] E.A. Batista, G.R.P. Malpass, A.J. Motheo, T. Iwasita, New mechanistic aspects of methanol oxidation, J. Electroanal. Chem. 571 (2004) 273–282, https://doi.org/10.1016/j.jelechem.2004.05.016.
[37] J. Kang, S. Nam, Y. Oh, H. Choi, S. Wi, B. Lee, T. Hwang, S. Hong, B. Park, Electronic effect in methanol dehydrogenation on Pt surfaces: potential control during methanol electrooxidation, J. Phys. Chem. Lett. 4 (2013) 2931–2936, https://doi.org/10.1021/jz401450v.
[38] Y.X. Chen, S. Ye, M. Heinen, Z. Jusys, M. Osawa, R.J. Behm, Application of in-situ attenuated total reflection-Fourier transform infrared spectroscopy for the understanding of complex reaction mechanism and kinetics: formic acid oxidation on a Pt film electrode at elevated temperatures, J. Phys. Chem. B 110 (2006) 9534–9544, https://doi.org/10.1021/jp057463h.
[39] G.L. Chiarello, D. Ferri, E. Selli, In situ attenuated total reflection infrared spectroscopy study of the photocatalytic steam reforming of methanol on Pt/TiO2, Appl. Surf. Sci. 450 (2018) 146–154, https://doi.org/10.1016/j.apsusc.2018.04.167.
[40] M. Li, P. Liu, R.R. Adzic, Platinum monolayer electrocatalysts for anodic oxidation of alcohols, J. Phys. Chem. Lett. 3 (2012) 3480–3485, https://doi.org/10.1021/jz3016155.
[41] H. Wang, H.D. Abruña, Origin of multiple peaks in the potentiodynamic oxidation of CO adlayers on Pt and Ru-modified Pt electrodes, J. Phys. Chem. Lett. 6 (2015) 1899–1906, https://doi.org/10.1021/acs.jpclett.5b00493.
[42] S.W. Lee, S.O. Chen, W.C. Sheng, N. Yabuuchi, Y.T. Kim, T. Mitani, E. Vescovo, Y. Shao-Horn, Roles of surface steps on Pt nanoparticles in electro-oxidation of carbon monoxide and methanol, J. Am. Chem. Soc. 131 (2009) 15669–15677, https://doi.org/10.1021/Ja9025648.
[43] S.W. Lee, S. Chen, J. Suntivich, K. Sasaki, R.R. Adzic, Y. Shao-Horn, Role of surface steps of Pt nanoparticles on the electrochemical activity for oxygen reduction, J. Phys. Chem. Lett. 1 (2010) 1316–1320, https://doi.org/10.1021/jz100241j.
[44] L. Yang, J. Ge, C. Liu, G. Wang, W. Xing, Approaches to improve the performance of anode methanol oxidation reaction—a short review, Current Opinion in Electrochemistry 4 (2017) 83–88, https://doi.org/10.1016/j.coelec.2017.10.018.
[45] Y. Liu, M. Muraoka, S. Mitsushima, K.-I. Ota, N. Kamiya, Electrochemical and ATR-FTIR study of dimethyl ether and methanol electro-oxidation on sputtered Pt electrode, Electrochim. Acta 52 (2007) 5781–5788, https://doi.org/10.1016/j.electacta.2007.02.061.
[46] L.W. Liao, S.X. Liu, Q. Tao, B. Geng, P. Zhang, C.M. Wang, Y.X. Chen, S. Ye, A method for kinetic study of methanol oxidation at Pt electrodes by

electrochemical in situ infrared spectroscopy, J. Electroanal. Chem. 650 (2011) 233–240, https://doi.org/10.1016/j.jelechem.2010.09.012.
[47] Z.-Y. Zhou, N. Tian, Y.-J. Chen, S.-P. Chen, S.-G. Sun, In situ rapid-scan time-resolved microscope FTIR spectroelectrochemistry: study of the dynamic processes of methanol oxidation on a nanostructured Pt electrode, J. Electroanal. Chem. 573 (2004) 111–119, https://doi.org/10.1016/j.jelechem.2004.07.003.
[48] C.S. Kim, W.J. Tornquist, C. Korzeniewski, Site-dependent vibrational coupling of CO adsorbates on well-defined step and terrace sites of monocrystalline platinum: mixed-isotope studies at Pt(335) and Pt(111) in the aqueous electrochemical environment, J. Chem. Phys. 101 (1994) 9113–9121, https://doi.org/10.1063/1.468040.
[49] D.K. Lambert, Vibrational Stark effect of adsorbates at electrochemical interfaces, Electrochim. Acta 41 (1996) 623–630, https://doi.org/10.1016/0013-4686(95)00349-5.
[50] E. Boscheto, B.C. Batista, R.B. Lima, H. Varela, A surface-enhanced infrared absorption spectroscopic (SEIRAS) study of the oscillatory electro-oxidation of methanol on platinum, J. Electroanal. Chem. 642 (2010) 17–21, https://doi.org/10.1016/j.jelechem.2010.01.026.
[51] A.M. Gómez-Marín, J.M. Feliu, Pt(111) surface disorder kinetics in perchloric acid solutions and the influence of specific anion adsorption, Electrochim. Acta 82 (2012) 558–569, https://doi.org/10.1016/j.electacta.2012.04.066.
[52] A. Björling, J.M. Feliu, Electrochemical surface reordering of Pt(111): a quantification of the place-exchange process, J. Electroanal. Chem. 662 (2011) 17–24, https://doi.org/10.1016/j.jelechem.2011.01.045.
[53] H. Tributsch, J.C. Bennett, Electrochemistry and photochemistry of MoS2 layer crystals, J. Electroanal. Chem. Interfacial Electrochem. 81 (1977) 97–111, https://doi.org/10.1016/S0022-0728(77)80363-X.
[54] H. Yano, T. Uematsu, J. Omura, M. Watanabe, H. Uchida, Effect of adsorption of sulfate anions on the activities for oxygen reduction reaction on Nafion®-coated Pt/carbon black catalysts at practical temperatures, J. Electroanal. Chem. 747 (2015) 91–96, https://doi.org/10.1016/j.jelechem.2015.04.007.
[55] T. Iwasita, Electrocatalysis of methanol oxidation, Electrochim. Acta 47 (2002) 3663–3674, https://doi.org/10.1016/S0013-4686(02)00336-5.
[56] S.C.S. Lai, N.P. Lebedeva, T.H.M. Housmans, M.T.M. Koper, Mechanisms of carbon monoxide and methanol oxidation at single-crystal electrodes, Top. Catal. 46 (2007) 320–333, https://doi.org/10.1007/s11244-007-9010-y.
[57] S. Wilhelm, T. Iwasita, W. Vielstich, Coh and Co as adsorbed intermediates during methanol oxidation on platinum, J. Electroanal. Chem. 238 (1987) 383–391, https://doi.org/10.1016/0022-0728(87)85187-2.
[58] T.R. Ralph, M.P. Hogarth, Catalysis for low temperature fuel cells part II: the anode challenges, Platin. Met. Rev. 46 (2002) 117–135.
[59] T. Iwasita-Vielstich, Progress in the study of methanol oxidation by in situ, ex situ and on-line methods, in: H. Gerischer, C.W. Tobias (Eds.), Advances in Electrochemical Science and Engineering, VCH Verlagsgesellschaf, Weinheim, 1990, pp. 127–170.
[60] Y.-P. Sun, L. Xing, K. Scott, Analysis of the kinetics of methanol oxidation in a porous Pt–Ru anode, J. Power Sources 195 (2010) 1–10, https://doi.org/10.1016/j.jpowsour.2009.07.028.